Technical Report
1049

19981001 082

Radar Determination of Turbulence Exceedance Probability

J.W. Snow
H.K. Burke
D.C. Peduzzi
C.A. Upham
M.P. Jordan

25 September 1998

Lincoln Laboratory

MASSACHUSETTS INSTITUTE OF TECHNOLOGY

LEXINGTON, MASSACHUSETTS

DTIC QUALITY INSPECTED 1

This technical report has been reviewed and is approved for publication.

FOR THE COMMANDER

Gary Tutungian
Administrative Contracting Officer
Contracted Support Management

Unclassified

MASSACHUSETTS INSTITUTE OF TECHNOLOGY
LINCOLN LABORATORY

RADAR DETERMINATION OF TURBULENCE EXCEEDANCE PROBABILITY

J.W. SNOW
H.K. BURKE
D.C. PEDUZZI
C.A. UPHAM
M.P. JORDAN
Group 97

LEXINGTON   MASSACHUSETTS

Unclassified

ABSTRACT

Modern high power Doppler VHF radar wind profilers are a valuable source of upper tropospheric turbulence intensity information. These radars can provide more comprehensive characterization of turbulence statistics than any in-situ measurement database, or even models developed from such data-bases. Sample data sets from two high power radar profilers, located at WSMR, New Mexico, and KSC, Florida, were obtained. The physical processes involved in turbulence production, maintenance, and dissipation were reviewed along with the phenomenology of its detection using radar. Subsequently, methodologies were developed for the retrieval of turbulence intensity statistics, or the so-called turbulence exceedance probabilities (TEP), from such data. The WSMR data analysis shows that, in the 8 to 20 km altitude region, the median turbulence intensity was ≤ 0.5 m s^{-1}. In more turbulent conditions, the 90% and 95% TEP, turbulence intensities were observed to be close to, or slightly in excess of 1.0 m s^{-1} and 1.5 m s^{-1}, respectively. The KSC turbulence data analysis resulted in the median close to 1.0 m s^{-1}, the 90% TEP near 1.5 m s^{-1}, and the maximum 95% TEP of 1.7 m s^{-1}.

Also considered are the capabilities of a recently developed Clear Air Turbulence (CAT) forecast product. The conclusion is that available TEP guidance could be validated and extended by analysis of data from high power radars.

TABLE OF CONTENTS

LIST OF ILLUSTRATIONS

Figure No.

LIST OF TABLES

1. INTRODUCTION

Unusually high values of turbulence intensity are of concern, especially to air operations conducted in the upper portion of the troposphere. The turbulence statistics of interest are the magnitude, frequency of occurrence, location, and spatial extent—vertical and horizontal—of such high turbulence situations. In view of the localized and transient character of severe turbulent events, in-situ measurements are not the ideal source for turbulence exceedance probability (TEP) statistics.

Vertical profiles of turbulence exceedance probability are available from the so-called "medium/ high altitudes TEP diagram," reproduced as Figure 1 (from Figure 7 or Figure 31, MIL-F-8785B or C, 1969 or 1980, respectively). These profiles were presumably generated from high-response pressure (pitot tube) measurements and have been relied upon extensively. They represent the environmental conditions of the geographic locations, altitudes, and seasons where the measurements were made and are subject to the characteristics of the in-situ measurement systems used. The enduring utility of this diagram attests to the magnitude of any effort at improvement. The recent development of radar wind profilers may warrant the reexamination of the available TEP guidance.
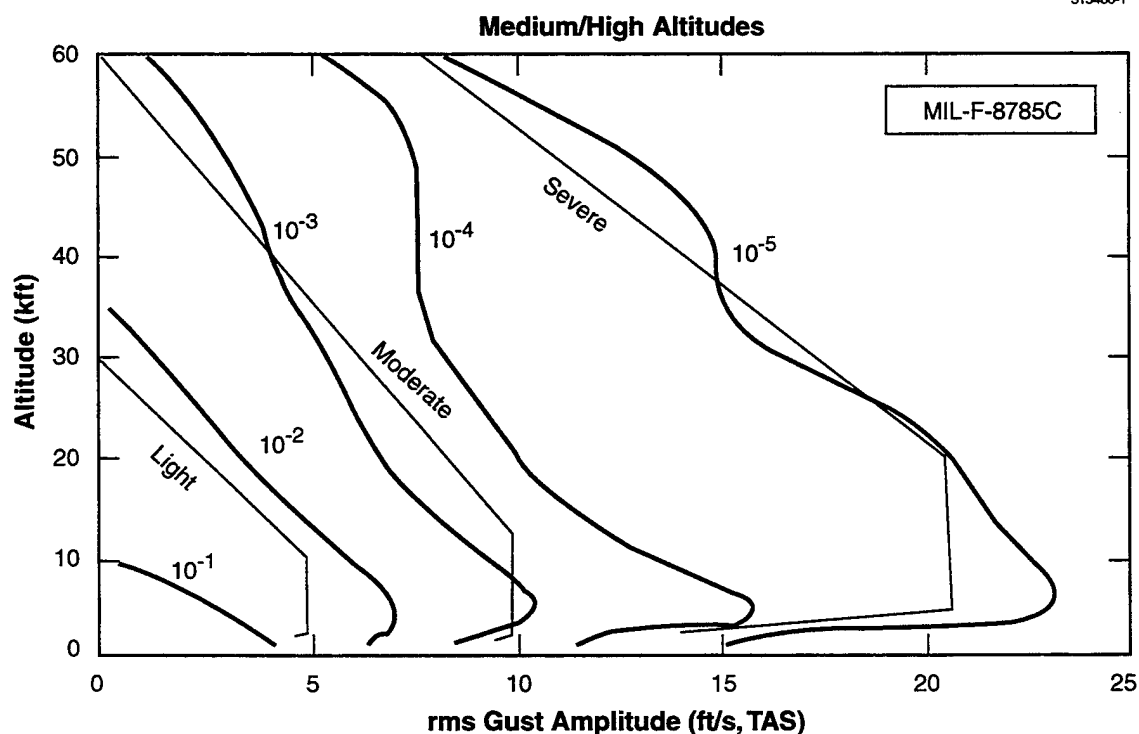
Figure 1. Turbulence exceedance probability (TEP) diagram. Turbulence intensity, same as rms gust amplitude σ_u (ft/sec) abscissa, versus altitude (kft). Bold profiles are TEP from in-situ (aircraft) assessment. Parameter is probability limit, 10^{-2} is 1-in-100 chance of exceedance. Lighter profiles are accepted model definitions of minimum threshold σ_u-values for stated intensity of clear-air turbulence. Diagram reproduced from: Military Specification — Flying Qualities of Piloted Airplanes, MIL-F-8785C, 5 November 1980.

1

Modern high power Doppler VHF radar sensing of the clear atmosphere provides remote quantification of turbulence intensity within the mesosphere, stratosphere, and troposphere, explaining the common name: MST radar. These VHF radars operate in the frequency range from 2 to 1000 MHz (wavelength range 150 m to 30 cm). Although large in physical size, and therefore deployed at fixed locations, they provide a continuous, homogeneous, and traceable database for evaluating atmospheric wind and turbulence conditions. They can now be used to confirm, refine, and extend the available turbulence guidance, the TEP diagram. High power VHF radar systems provide the only comprehensive coverage within the upper tropospheric layers—a region characterized by strong wind shear that is vertically isolated, horizontally localized, and transient.

Samples of such data from two separate VHF radars were analyzed in support of the Maneuverable Towed Countermeasure Dynamics (MTCD) Program. Some physics of atmospheric turbulence is considered in Section 2 and the applicability of VHF radar as a measurement tool is discussed in Section 3. Details of the turbulence intensity retrieval algorithms are given in Section 4 and associated error sources are discussed in the Appendix. Section 5 explains the radar data sets analyzed and the summary wind and turbulence statistics are presented. The available data sets were searched for especially turbulent atmospheric conditions; the results are shown in Section 6. A recently developed methodology which provides clear-air turbulence forecasts by processing the output information from numerical weather prediction models is discussed in Section 7. These results are summarized in Section 8 and some implications of VHF radar assessment of turbulence and of turbulence forecast utility are discussed.

2. TURBULENCE INTENSITY

Understandably, turbulence intensity, here quantified by the rms wind velocity σ_u (m s^{-1}), and airframe velocity fluctuations (commonly called 'buffeting' or 'turbulence') are proportional to each other, since the former is the environmental cause of the latter. The magnitude of the average wind 'gust' is the meaning of σ_u, and σ_u is in fact the abscissa of the TEP diagram. The wind variance σ_u^2 (m^2 s^{-2}) is also often used to quantify turbulence. Specifically, σ_u^2 is the measure of the kinematic momentum flux, and 1/2 σ_u^2 quantifies the turbulent kinetic energy per unit mass of air, which is assigned the symbol K (m^2 s^{-2}). More precisely, K is 1/2 of the wind vector variance, providing for the three independent and orthogonal components of the fluctuating wind (u, v, w), which results in K = 1/2 $[\sigma_u^2 + \sigma_v^2 + \sigma_w^2]$. For the spatial scales where radar detects turbulence, all components are equal (the isotropic turbulence condition) and therefore, K = 3/2 σ_u^2. (The u-component is used generically.) If a single component dominates, a condition thought to exist during turbulence production, then K = 1/2 $(\sigma_u^2 + \delta) \cong$ 1/2 σ_u^2, $\delta \ll 1.0$.

The K-budget equation (Stull, 1988, Equation 5.1) contains various source (time-rate-of-production) and sink (consumption, dissipation) terms along with local storage and various transport terms. Traditionally, turbulence theory applies to the atmosphere's bottom boundary layer, near the surface. Allowing for physical differences, but with useful authenticity, the theory can be applied near the 'boundary' at the top of the troposphere, the tropopause. Some K-budget terms, which near the surface may be large and diurnally varying, are negligible. Others, like net vertical transport which may be small near the surface, are predominant near the tropopause.

The tropopause is the level at which decreasing temperature, characteristic of the troposphere, ceases and is replaced by isothermal or increasing temperature within the lower stratosphere. Also, high in the troposphere, especially at middle-latitude locations, maximum wind speeds—jet streams—are found. These are caused by large-scale horizontal temperature gradients which are not directly eliminated by the atmospheric motions because of the effects of earth's rotation. Jet streams are a common source of turbulent kinetic energy and are often associated with intense turbulence. The profiles of mean wind speed and temperature in the vicinity of the tropopause are schematically represented in the first panels of Figure 2a.

The principal terms in the K-budget equation near the tropopause are: 1) production of K by vertical wind shear, mostly on the tropospheric side, 2) consumption by the stable stratification on the stratospheric side, 3) turbulent vertical transport from below to above the tropopause, and 4) the possibility for larger-scale vertical redistribution by gravity waves. The first three of these are shown in the third panel of Figure 2a.

Commonly, shear in the wind, especially vertical shear, is the source of turbulent kinetic energy. Production of K occurs with the formation of large, mostly horizontal rolls, i.e., vortices, within the shearing flow. Above the surface boundary layer, local change (storage) and mean advection are often negligible. This equilibrium condition is then temporally stationary and horizontally homogeneous (Meecham, 1972). Although horizontal transport terms are mutually canceling, their activity may be important to clear-air radar measurement of turbulence intensity. Net vertical transport of turbulent kinetic energy ($\Delta K/\Delta z\ \Delta z/\Delta t$) is a major term and is explicitly shown in Figure 2a. Horizontal transport

3

is only implicitly indicated, i.e., near the level of maximum wind speed, production is seen to equal consumption.
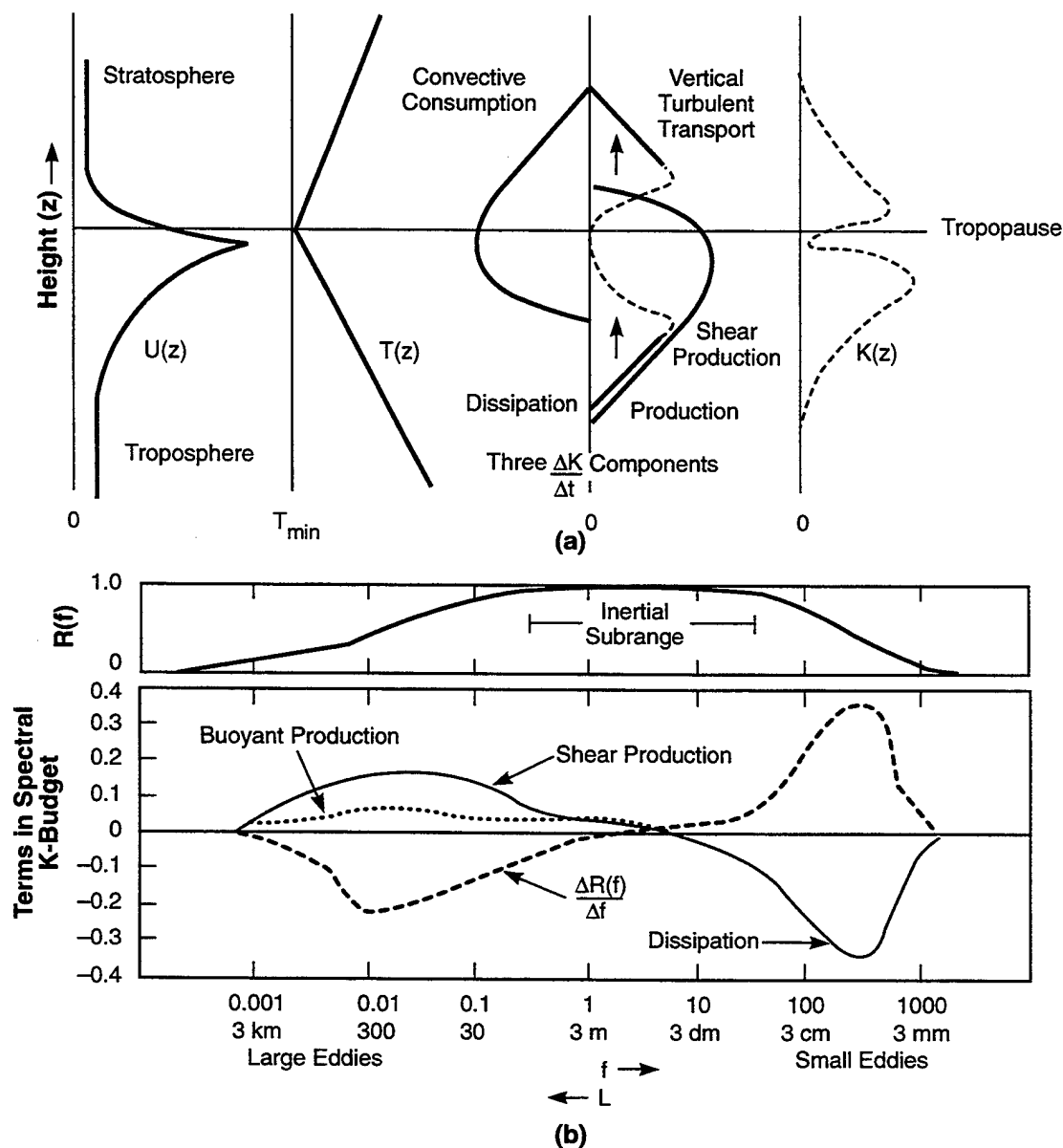
Figure 2. Schematic of principal components in turbulent kinetic energy budget $\Delta K/\Delta t$, (a) in vicinity of tropopause, and (b) in the spectral domain. (a) Profiles of mean wind U, temperature T, three K-budget terms, and turbulent kinetic energy K. (b) Spectral transfer rate $R(f) = \Delta K/\Delta f \, \Delta f/\Delta t$, three K-budget terms in spectral domain, and negative sum of terms $\Delta R(f)/\Delta f$. Normalized spatial frequency $f = \pi/L$, L is eddy size.

4

The final term in the K-budget equation, the viscous dissipation ε, which is the rate of conversion of K into heat, is only being carried out by the smallest dynamic entities, minute vortices or eddies of dimension 1 cm. In Figure 2a it is represented as convective consumption which is acting to accomplish warming of the coldest air located at the tropopause. This dissipation occurs isotropically, in contrast to K production. More generally, the sizes of eddies effecting each function (production, transport, dissipation) vary and the topic of spatial scales needs further consideration.

Within a range of eddy sizes ΔL or equivalently spatial frequencies Δf, called the inertial-subrange, the Kolmogorov conditions are assumed to prevail. Specifically, the magnitude of K and the rate at which it is transferred spectrally R are approximately conserved. R is the rate at which K is passed down from larger to smaller eddies. In the inertial-subrange, R $(m^2 \, s^{-3}) = \Delta K/\Delta t$, is nearly constant. Figure 2b (adapted from Stull, 1988, Figure 5.16) contains the spectral depiction of R and the major K-budget terms—production (both by shear and buoyancy) at large scales, dissipation at small scales, and spectral transfer at intermediate scales, i.e., within the inertial-subrange.

The extent ΔL of the inertial-subrange in the atmosphere generally varies with density (and therefore decreases with height), and narrows with increasing thermal stability (refer to Hocking, 1985, Figure 1). Within the upper troposphere, the inertial-subrange is about 1 cm to 100 m, and in the lower stratosphere, 10 cm to 10 m. The inertial-subrange depicted in the top panel of Figure 2b corresponds closely to the tropospheric extent. For the radar detection of turbulence intensity what is significant is that, within this subrange, production and dissipation are negligibly small, the spectral transfer is maximum and nearly constant, and therefore K itself is nearly constant. Therefore, K measured at any scale within ΔL is the same.

The turbulent energy dissipation rate per unit mass ε $(m^2 \, s^{-3})$ occurs primarily at scales < 1 cm, and as seen in Figure 2b it is essentially zero within the inertial-subrange. Nevertheless, as given in Section 3, ε can be related to the inertial-scale turbulence parameter—the rms wind velocity σ_u—because of the conservation of K throughout the inertial-subrange. (Even relating ε to the much larger-scale wind shear, in the K-production range, is a possibility, one that VHF radar could assist in.) Because of the Kolmogorov conditions, many small and large scale turbulence parameters can be directly related. The useful result is that assessment of turbulence intensity made at a smaller scale, particularly by a VHF radar, has direct and valid applicability to other larger scale sizes, specifically that of an aircraft or of any airframe and its extended environment.

3. RADAR DETECTION OF TURBULENCE

The physical reason why VHF radar can detect clear-air turbulent fluctuations is now considered, as are the two methods by which Doppler radar can quantify the turbulence magnitude—the backscatter power and the spectrum width methods.

VHF radar data can provide vertical profiles of wind speed and turbulence intensity from analysis of range-resolved backscattered signal. The size of the detected atmospheric entities, the eddies generating the backscattered energy, are characteristically $\lambda/2$, where λ is the transmitted radar wavelength (Hardy, 1972). Thus, for a 50 MHz radar, eddies of size 300 cm (3 m) are the primary source of backscattered signal. This is well within the inertial-subrange throughout the troposphere, stratosphere, and mesosphere up to nearly 70 km. From Figure 2b, at 3 m, all K-budget terms are small except the spectral transfer R; this term must therefore be responsible for the backscattered radar signal. In the middle of the inertial-subrange are "larger eddies creating or bumping into smaller ones, and transferring some of their inertia in the process" (Stull, 1988, p. 167). A dynamic equilibrium of density gradients is thereby generated, which is called index of refraction fluctuations $\Delta n/\Delta t$ in the radar literature, and is responsible for scattering radar energy.

Determining profiles of wind speed involves assessing the Doppler shift of returned versus transmitted energy as a function of range. For the mean wind speed profile, a tunable broad-band receiver is sufficient. In contrast, for turbulence intensity evaluation, two distinct methods are employed, both of which require more complex receivers. These are analysis of the magnitude or analysis of the spectrum of the returned signal. The vertical resolution of radar profile data, for either mean wind or turbulence analysis, is determined by the radar transmitter power—stronger return from a minimum number of backscattering eddies within a radar volume.

Within the inertial-subrange the nearly constant R results in a nearly constant rms wind velocity, which can be shown (Tatarski, 1961, p. 29) to be a function to the third-root of the turbulent energy dissipation rate, specifically, $\sigma_u \sim \varepsilon^{1/3}$. Also, $\varepsilon^{1/3}$ is proportional to the rms of the atmospheric refractive index structure parameter σ_n, and $\sigma_n^2 = C_n^2$, a definition. C_n^2 is due to the atmospheric density fluctuations $\Delta\rho/\Delta t$ caused by R. C_n^2 is itself directly proportional to the magnitude of the radar-volume backscatter power η. Therefore, the magnitude of backscatter power, the refractive index structure parameter, and the wind variance are all related, specifically, $\eta \sim C_n^2 \sim \sigma_u^2 \sim \varepsilon^{2/3}$. This relationship is used in the original VHF radar turbulence intensity technique, the η-method. The magnitude of the broad-band radar returned power—that back-scattered by $\lambda/2$-sized eddies of differing densities and therefore differing refractive indices—is the signal. A number of environmental factors other than σ_u^2 can contribute to η and these need to be considered before backscatter power is used as a reliable measure of turbulence intensity. These error sources are considered in the Appendix.

An alternative, more direct and possibly more accurate method uses a sensitive Doppler radar receiver to generate the spectrum of return signals during an appropriate integration time by all $\lambda/2$-sized eddies within the radar volume. These eddies are moving with various 'gust' speeds superimposed upon the mean wind. Physically, the individual received signals are Doppler-shifted about the fixed-frequency

7

of the transmitted pulse by the motion, relative to the transmitter, of each $\lambda/2$-sized backscattering eddy. The frequency distribution of signals received from a train of individual fixed-wavelength transmitted pulses is a direct representation of two constituents of the atmospheric motion: the mean wind speed and the rms velocity of these eddies, in the direction toward and away from the transmitter. The displacement of the overall spectrum from the transmitter frequency is a measure of the mean wind. The half-power half-width of the measured return spectrum ϕ_m is related to the fluctuating density caused by the eddy rms motion, and therefore to the turbulence intensity. As before, turbulence intensity is related to the energy dissipation rate, but now, $\phi_m \sim \sigma_u^{3/2} \sim \varepsilon^{1/2}$. This is the basis for the other clear-air radar turbulence quantification method, referred to here as the ϕ-method. However, as discussed more in the Appendix, corrections to ϕ_m for spectrum broadening caused by the mean horizontal wind, its vertical shear, and by radar system parameters must always first be made.

4. TURBULENCE ASSESSMENT METHODOLOGIES

The procedures for applying the two methods of determining turbulence intensity profiles from VHF radar data are summarized at the end of the section, in Table 1. The equations themselves are developed below. The retrieval of turbulence intensity, by either method, takes advantage of the quasi-steady state of turbulence within the inertial subrange, the spatial frequency range where VHF radar senses. In that range of atmospheric eddy sizes, both generation and dissipation of turbulence are minimal. Since the physics is simpler, the retrieval algorithms are inherently more robust.

4.1 Backscatter Power

The transformation of VHF radar data to profiles of σ_u, directly comparable to the TEP diagram, or more correctly, to the individual σ_u-values from which the exceedance statistics were derived, involves the specific relationship between σ_u and $(C_n^2)^{1/2}$. Required are representative values of environmental variables and radar system parameters. This expression is developed using previous research at MIT Lincoln Laboratory (Labitt, 1981) and at the DOC, Wave Propagation Laboratory (Gage et al., 1980). Specifically,

$$\sigma_u(z) = A \ [T(z)/p(z)] \ (C_n^2)^{1/2} \ (r)^{1/3}$$

where T, p are environmental temperature and pressure as functions of height z, A is a constant, and r is the range which is equal to height z for vertically pointing radar.

Following Gage et al. (1980, p. 410, Eq. 10), for the 'dry' atmosphere, namely above 8 km, the turbulent energy dissipation rate at height z is

$$\varepsilon(z) = 3.43 \times 10^{15} \ [(T(z)/p(z)) \bullet (1/F_N)^{1/2}]^3 \ (C_n^2)^{3/2}$$

where F_N (the third-root of the 'turbulent fraction' times the square of Brunt-Vaisala frequency) has been found from analyses of environmental data (VanZandt et al., 1978) to have two approximately constant values: a tropospheric value of 45×10^{-6} s^{-2} and a stratospheric value of 100×10^{-6} s^{-2}. (The overall topic of various error sources is considered in the Appendix.) The resulting expression (as in Hocking, 1985, p. 1413, Eqs. 41 and 42), applying the relatively 'constant' tropospheric and stratospheric values of F_N,

$$\varepsilon(z) = \gamma \ (T(z)/p(z))^3 \ (C_n^2)^{3/2}, \quad \varepsilon^{1/3} = \gamma^{1/3} \ (T/p) \ (C_n^2)^{1/2}$$

where $\gamma = 10.80 \times 10^{21}$ in the troposphere, 3.26×10^{21} in the stratosphere, giving ε in mks units (m^2 s^{-3}). Since it is $\varepsilon^{1/3}$ that is proportional to the turbulence intensity σ_u, then these 'constants' (the values of $\gamma^{1/3}$) become 2.21×10^7 in the troposphere and 1.48×10^7 in the stratosphere. In practice, the location of the upper-tropospheric wind speed maximum in the profile is a useful general indication of the tropopause height. Furthermore, a linear interpolation of the 'constant' between the two values is made within a 2-km transition layer. For the radar data discussed in detail in Section 5 which are analyzed using the η-method, the specific 2-km layers were 13–15 km (June 91) and 11–13 km (February 93).

9

LaBitt (1981, p. 3, 33, Eq. 10) relates the intensity of turbulence and $\epsilon^{1/3}$, in cgs units, by

$$\sigma_u(z) = 1.352 \; [\epsilon(z) \; W(z)]^{1/3} \; (\mathfrak{I})^{1/2}$$

where $\mathfrak{I}$, is a geometric factor having a small range of values between 0.92 and 1.00, which in the average gives $(\mathfrak{I})^{1/2} \cong 0.98$. W is the beamwidth dimension which varies with range and therefore z, $W = 2z \tan (\beta/2)$, β being the angular beamwidth—here taken to be 3.3°. The resulting expression is

$$\sigma_u(z) = 5.118 \times 10^{-1} \; [\epsilon(z) \cdot z]^{1/3}$$

where the unit for z must be (cm) and those for σ_u are (cm s^{-1}) in order for ϵ to remain in cgs units (cm^2 s^{-3}). Since a factor equal to the third-root of 10^5 is needed to enable km rather than cm to be used for the value of z, and, further, using an mks-units for ϵ in this expression requires multiplication of the coefficient by the third-root of 10^4; the net result is a simple change of the coefficient's exponential factor from 10^{-1} to 10^2. It is noted that the resulting σ_u-value is still in cgs units; conversion to mks is done with division by 10^2. Finally, as in Table 1,

$$\sigma_u(\text{m s}^{-1}) = 5.118 \; \epsilon^{1/3} \; (z(\text{km}))^{1/3}$$

4.2 Spectrum Width

The Doppler-shifting of the frequency (Δv) of backscattered radar energy contains information on σ_u along with that from various other factors, system and atmospheric, which cause frequency shifts in return signals. Important among the factors contributing to Δv, in addition to turbulence, are: specular reflection, mean horizontal motion across a finite beamwidth, vertical wind-shear within a finite radar range-gate, and temporal changes during the integration time (refer to the Appendix for details). An illustration of the overall effect of these factors is given in Hocking (1983b, p. 109, Figure 7). The result is that the lower limit on reliable determination of turbulence intensity σ_u is set by the ability to quantify and eliminate the effects of these other factors. In all cases this lower limit is non-zero and therefore the use of return spectrum data for specifying the central-moments, mean or median, of turbulence intensity is biased due to non-inclusion of the true number of low turbulence intensity cases. However, the high turbulence occurrences are well measured and, once any specular reflection error is eliminated, spectrum analysis is a valid and appropriate technique for developing accurate TEP statistics.

This ϕ-method is applied to a large data sample in Section 5. The spectral width values, the ϕ's, as they appear in the individual data records are analyzed directly. Thus, it is assumed that quality assurance, by elimination of the various system and environment errors, has already been carried out (procedures in accordance with Hocking, 1983a, p. 100, Table 1). In effect, the individual measured spectrum widths ϕ_m are reduced by the amount due to extraneous errors ϕ_e,

$$\phi_t^2 = \phi_m^2 - \phi_e^2$$

Also, in the large data sample used in Section 5, the corrected turbulence spectrum widths, the ϕ_t-values (Hz), are already converted to turbulence intensity σ_u (m s^{-1}). The conversion to turbulence intensity has been made, presumably, using the relationship derived by Hocking (1983a, p. 98, Eq. 47).

10

That is,

$$\sigma_u = \{[(\lambda/2)^2 \, (\phi_t^2)]/2 \, \ln \, (2)\}^{1/2}$$

where λ is the radar transmitter wavelength. The expression, $\sigma_u^2 = \sigma_m^2 - \sigma_e^2$, is sometimes more convenient to apply, where σ_e^2 is the portion of the measured variance σ_m^2 attributable to errors.

To summarize the turbulence assessment methodologies, the conversion of raw radar backscatter measurements to turbulence intensity, using either method, involves 1) the step-wise elimination of a number of error sources, and 2) the implementation of a retrieval algorithm. The major error sources are enumerated and the techniques for their elimination are indicated in the Appendix. In particular, the backscatter power (the η-method) is especially prone to water vapor contamination and to singularities in the temperature profile. The ϕ-method relies upon the elimination of spurious spectrum broadening, inevitably resulting from the finite size of radar sampling volumes, and of erroneous spectral peaks caused by specular reflection. Nonetheless, high power VHF radar affords good quality continuous measurement of upper tropospheric turbulence, and at superior vertical resolution. The two retrieval algorithms developed are ready to be applied.

TABLE 1

Summary of Methods for the Radar Determination of Turbulence Intensity

---

1. η-Method—Magnitude of Backscatter Power

    Basically, $\sigma_u(z) = A \, \varepsilon^{1/3} \, (z)^{1/3}$,

    A - constant = 5.118 for σ_u (m s^{-1}) and z (km),

    ε - turbulent energy dissipation rate,

    z - height, the radar range ÷ secant (beam zenith angle).

    But $\quad \varepsilon^{1/3} = \gamma^{1/3} \, (T/p) \, (C_n^2)^{1/2}$,

    γ - environmental lapse rate parameter: troposphere or stratosphere,

    T/p - environmental temperature/pressure profile values,

    C_n^2 - refractive index structure function (spatial variance).

    And $\quad C_n^2 \sim \eta$, the magnitude of backscatter power.

2. ϕ-Method—Doppler Broadening of Backscatter Spectrum

    Basically, $\sigma_u(z) = B \, (\lambda/2) \, \phi_t(z)$,

    B - constant = $[2 \ln (2)]^{-1/2}$

    λ - radar wavelength (600 cm),

    $\phi_t(z)$ - half-power half-width.

    But $\quad \phi_t^2 = (\phi_m^2 - \phi_e^2)$, 't' turbulence, 'm' measured, 'e' extraneous.

    And $\quad \phi_e^2$ is function of environmental factors and system characteristics.

11

5. RADAR PROFILE DATA

A number of near-vertical pointing VHF radars are now in use as wind profilers (NOAA, 1994). Two VHF radars within the United States have distinctively high peak power, 250 kW. The high power, along with more conventional receiver technology, allows short pulse duration and therefore high vertical resolution, 150 m. The parameters of these 50 MHz high power radars are contained in Table 2 (from Nastrom and Eaton, 1995). One is located at White Sands Missile Range (WSMR), New Mexico, and the other identical wind profiler is located at Kennedy Space Center (KSC), Florida. The locations are opportune; one being in mountainous mid-latitude terrain, the other in a flat subtropical region. Sample data sets from both profilers were obtained and analyzed. Each set was pre-processed elsewhere and both contained wind speed profiles. However, neither was complete enough for both turbulence assessment methods to be applied. The WSMR data sets are therefore analyzed by the η-method, the KSC using the ϕ-method.

TABLE 2

High-Power 50 MHz VHF Radar Parameters
(Manufacturer: Tycho Technology, Inc.)

TRANSMITTER:	
Nominal frequency	49.25 MHz (609 cm)
Output power	250 kW, peak
Duty cycle	5 %
Pulse width	8 μs
Compressed width	1 μs
Transmitter type	3-stage, solid-state preamp and tube-cavity amplifier
ANTENNA:	
Physical aperture	15,600 m^2
Effective aperture	13,500 m^2
Type	Coaxial-collinear phased array
Pointing	3-beam: zenith, 15° east, 15° north
Beamwidth	2.9°, one-way
RECEIVER:	
Type	Superheterodyne, low-noise
Bandwidth	Transmitter pulse matched
Noise	< 1 dB
PERFORMANCE:	
Lowest range-gate	2 km above ground
Range-gate resolution	150 m
Number of range-gates	112
Time resolution	1 min per beam
Wind speed range	± 116 m s^{-1}
Calibrated* C_n^2 range	10^{-20} to 10^{-13} m$^{-2/3}$
Bandwidth	1 MHz
Power-aperture product	1×10^8 W m^2
*WSMR radar only.	

The WSMR data are from all days during June 1991 and February 1993 and are 3-minute average values, every 5 minutes (12 per hour), of a 3-variable set—two orthogonal horizontal mean wind components, and C_n^2—within 100 range-gates (each of vertical extent 150 m) from 4.5 to 19.5 km. The total number of 3-variable sets at each range-gate is more than 8,000 (approximately $12 \times 24 \times$ # of days in each month). Summaries of the wind and turbulence intensity statistics developed from these WSMR data are contained in the profiles of Figures 3 and 4 for the altitude region 8 to 20 km. Data between 4.5 and 8 km are not analyzed due to atmospheric water vapor contamination (refer to the Appendix).

The profiles of wind speed, Figures 3a and 4a, present the median as the typical value. These are, then, profiles of the 50% (1-in-2) probability of exceedance, which is consistent with other turbulence quantifications. However, the median is not wholly comparable with the more common central-moment for wind, the mean wind, since wind speed usually has a positively skewed distribution, i.e., mean > median. For the two months studied, the height and magnitude of the maximum in the median wind speed profile do not differ significantly from published mean values for WSMR (taken from NOAA summary of radiosonde data, CD-ROM, 1995).

The profiles of wind statistics for the two month, Figures 3a and 4a, are representative of WSMR, in particular, of the seasonal variation to be expected in the southwest United States. There the winter-time jet stream is expected to be stronger and to be located at a lower altitude than the summer jet. From the median profiles in Figures 3a and 4a, this is seen to occur; the February maximum is 47 m s^{-1}, located near 10 km, versus the June value of 17 m s^{-1}, near 12 km. What is important about these wind analyses are the wind speed exceedance profiles, 90% (1-in-10) and 95% (1-in-20). In both seasons the occurrences of strongest winds are found near 10.5 km.

Profiles of median turbulence intensity and of the 90% and 95% turbulence exceedance probabilities (TEP) are presented in Figures 3b and 4b for the two months analyzed. The observed TEP profile maxima, during both months, are located on the upper side of the jet stream core. This is different from the schematic diagram of turbulent kinetic energy K(z), in Figure 2a, where the region immediately below the jet maximum is indicated as the location of most turbulence. However, due to the short period of the WSMR data here analyzed, no final conclusion can be made. The increase in the TEP values between 17 and 18.5 km during June is likely attributable to wind shear, whereas the near-linear increase in that region during February is probably due to persistent temperature gradients not compatible with the η-method retrieval algorithm (see Table A-1 in the Appendix).

Seasonal variations in the mean turbulence intensity profiles for WSMR have been developed by Nastrom (1995) and are reproduced in Figure 5. The values plotted are three-month averages of hourly-mean values of σ_u. The median profiles of Figures 3b and 4b are consistent with these much longer-term statistics—the period of data for Figure 5 is three years. In this regard, it should be noted that the variations about the seasonal means, shown in Figure 5 as line segments of $\pm$ 1 standard-error-of-mean plotted every 750 m, are formed from standard deviations of hourly-mean values of σ_u, and not of individual σ_u-values. The true extent of variations is therefore minimized.

14

Wind Speed Statistics, WSMR, June 1991

(a)

Turbulence, WSMR, June 1991

(b)
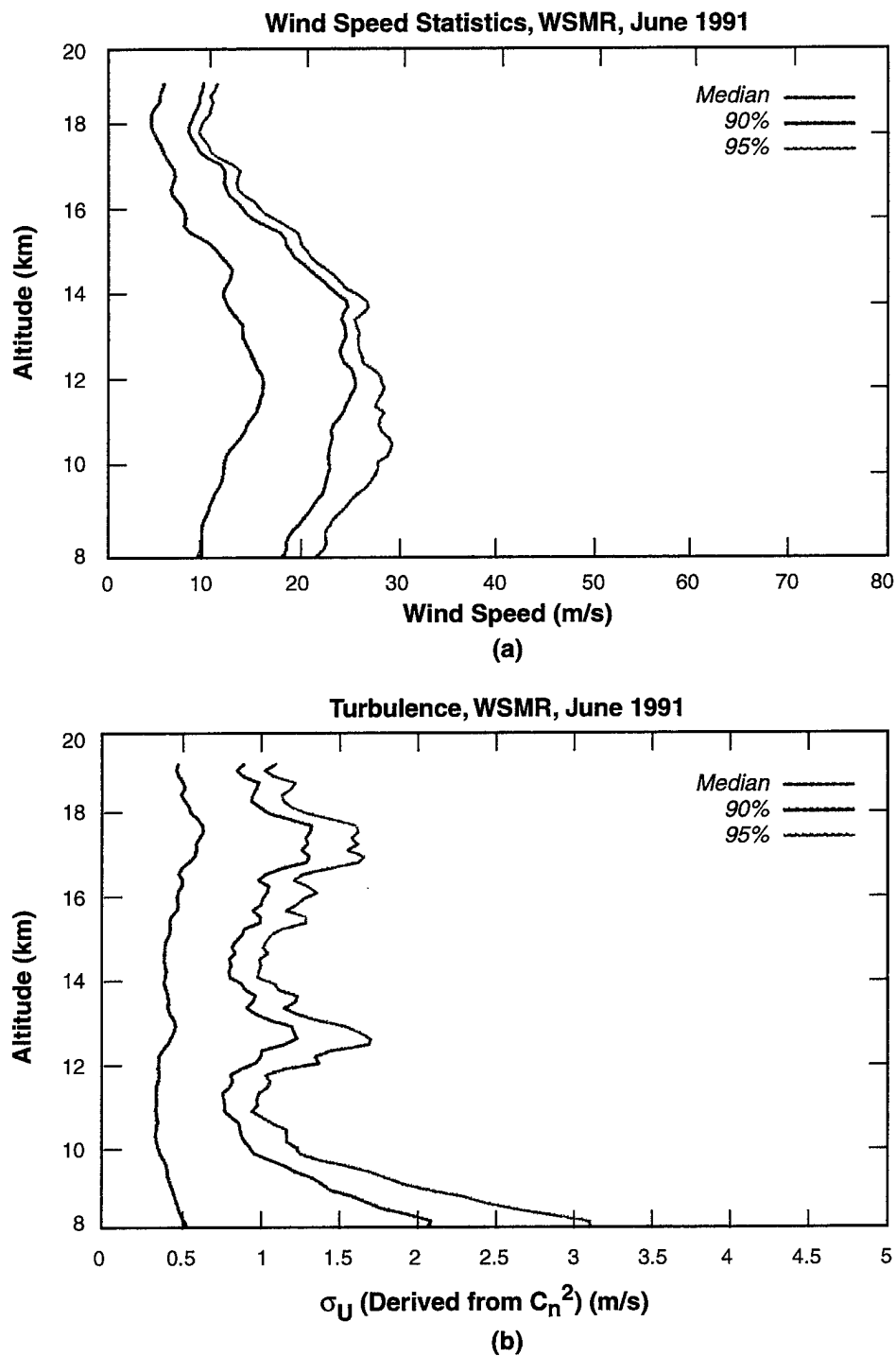
Figure 3. Profiles of (a) wind speed and (b) turbulence intensity statistics for June 1991 at White Sands Missile Range, New Mexico. Green curves are (a) median wind speed and (b) median turbulence intensity. Blue and red curves are probability of exceedance limits, 90% (1-in-10) and 95% (1-in-20), respectively. Statistics developed from 50 MHz high power radar data of altitude resolution 150 m, one profile every 5 minutes for 30 days.

313486-4B

Wind Speed Statistics, WSMR, February 1993

(a)

Turbulence, WSMR, February 1993

(b)

Figure 4. Profiles of (a) wind speed and (b) turbulence intensity statistics for February 1993 at White Sands Missile Range, New Mexico. Green curves are (a) median wind speed and (b) median turbulence intensity. Blue and red curves are probability of exceedance limits, 90% (1-in-10) and 95% (1-in-20), respectively. Statistics developed from 50 MHz high power radar data of altitude resolution 150 m, one profile every 5 minutes for 28 days.
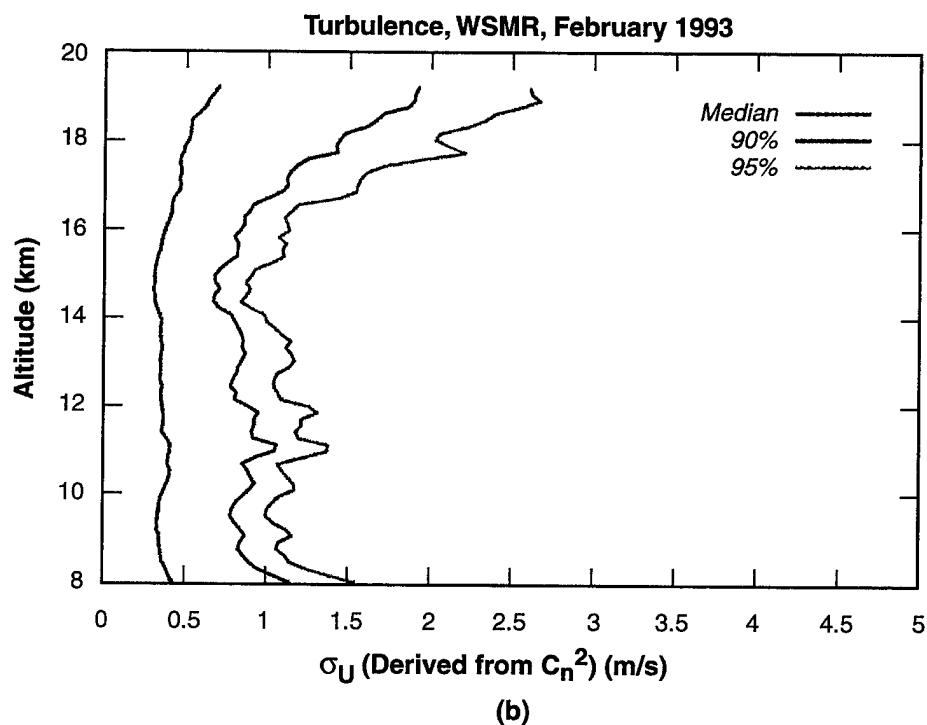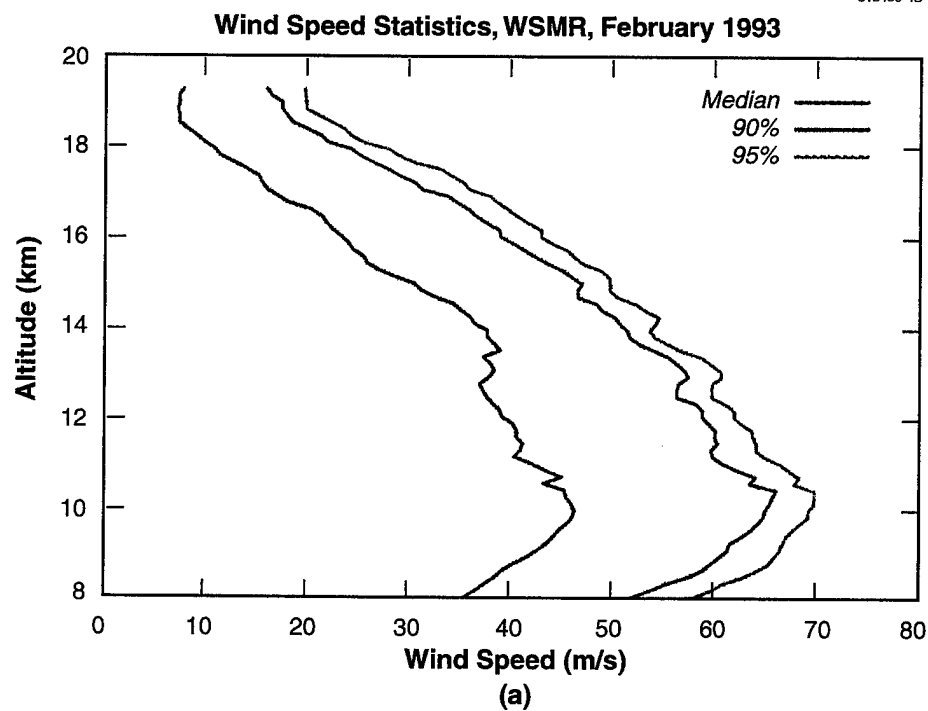
The sample data from KSC, for the period 1 October 1995 to 31 March 1996, consist of information from each of the three synthetic beams of the 50 MHz system: the vertical, eastward tilting, and northward tilting. Beamwidth is nominally 5° for all KSC beams (ENSCO, 1992) and the off-zenith angle for both tilted beams is 15°. The sample data set consists of more than 30,000 individual vertical profiles, generated every five minutes throughout the data-period (intermittent gaps constituting nearly 20,000 profiles). The profiles extend from 2 to 19 km at a vertical resolution of 150 m, but again, only the portions above 8 km were analyzed. An individual data record is available for each vertical range interval (height above mean sea level) of each profile. The individual data record contains height, 3-min mean horizontal wind direction and speed, and vertical speed, followed by the return signal power for each of the three beams, noise level, and spectrum width. As explained in Section 4.2, the spectrum width can be expressed as turbulence intensity σ_u (m s^{-1}) rather than as spectral range of frequency Δv (Hz). The KSC spectrum width data are so expressed. The specific width corrections are not known.

The entire six-month period of available KSC profile data are analyzed together since they all represent the low-sun season in the subtropical climate of KSC. Only the tilted-beam data records are analyzed, since they contain horizontal wind speed information. The resulting wind and turbulence profiles are contained in Figure 6. The median wind speed profile and the wind exceedance probability profiles are given in Figure 6a for the 90% (1-in-10), and the 95% (1-in-20) limits. Here the subtropical jet stream, located near 12 km, accounts for the strongest winds.

The median turbulence intensity profile (the 50% TEP limit) and the TEP profiles for the 90% and 95% limits are given in Figure 6b. Two features of these profiles are considered. First, the overall turbulence profile shape is similar to that of the wind itself, i.e., concave-left. This is in contrast to the WSMR cases, Figures 3 and 4, where the turbulence profiles are basically concave-right. The KSC shape is probably more correct, at least in the tropospheric region where water vapor can occur. As pointed out in the Appendix, the ϕ-method, applied to the KSC data, is minimally sensitive to water vapor contamination, whereas the η-method is extremely sensitive to it. Secondly, the overall value of the KSC median intensity is nearly 1.1 m s^{-1}, a high value. This is no doubt due to incomplete removal of all error sources. The net effect is a systematic overestimation of the smaller σ_u-values and relatively little modification of larger values. Thus, the 90% and 95% TEP profiles are more accurate than the median (50%) profile.

17
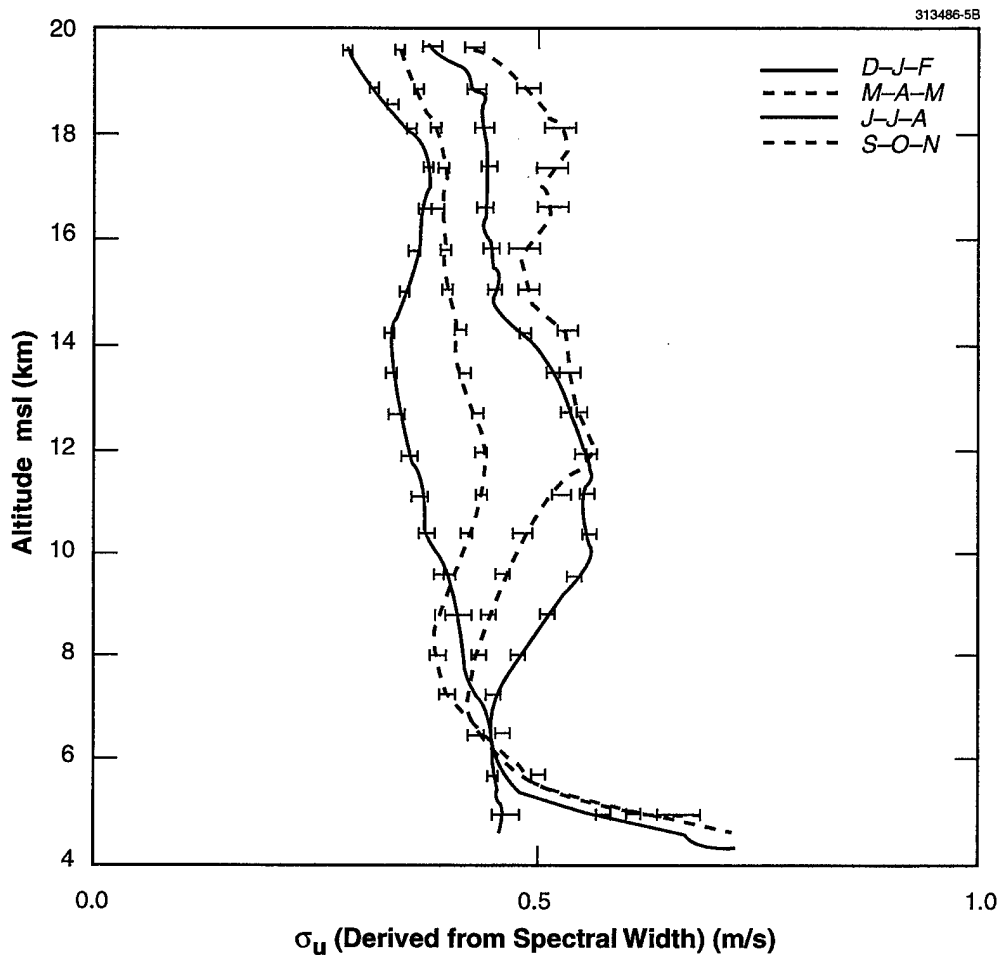
Figure 5. Seasonal mean profiles of hourly-averaged turbulence intensity σ_u from zonal (east-west) beam of WSMR 50 MHz radar data during the period January 1991 through April 1994. Means are developed from hourly average values of measured spectral half-power half-widths. Values are formed by averaging all mean-hourly σ_u-values, at each 150 m height-interval, during each 3-month season. Variation about seasonal means (±1 std. dev.) shown by line segments every 750 m. (From Nastrom, 1995.)

18

313486-6B

Wind Speed Statistics, KSC, October 95 – March 96

Median ————
90% ————
95% ————

Altitude (km) vs **Wind Speed (m/s)**

(a)

Turbulence, KSC, October 95 – March 96

Median ————
90% ————
95% ————

Altitude (km) vs **σ_U (Derived from Spectral Width) (m/s)**

(b)
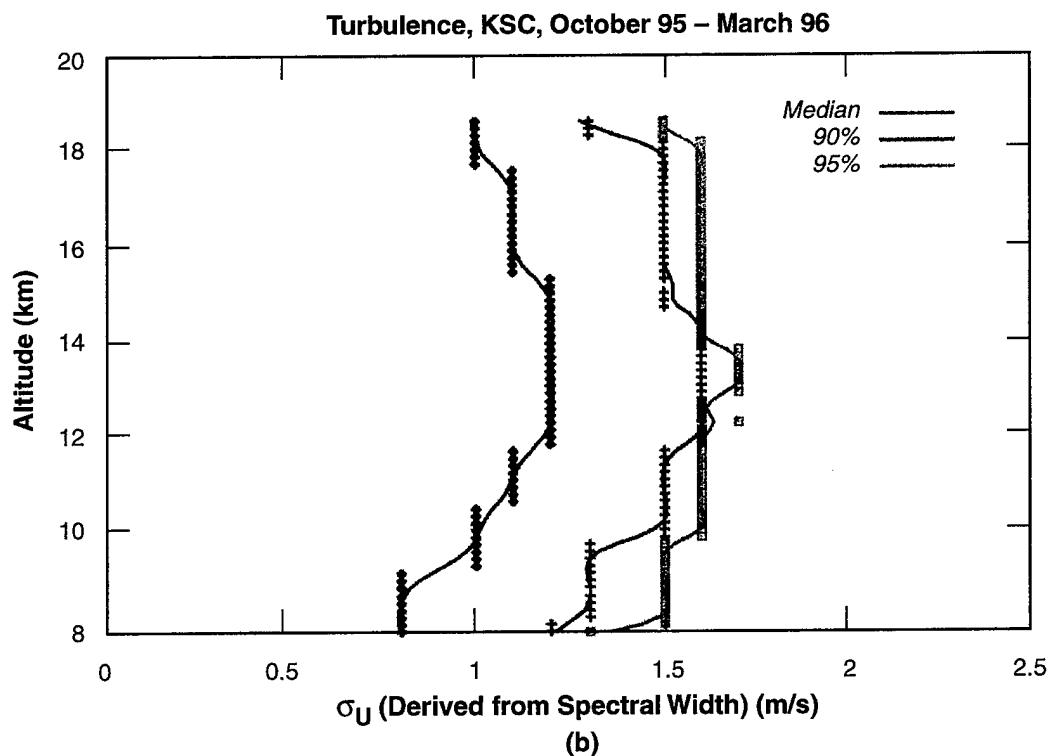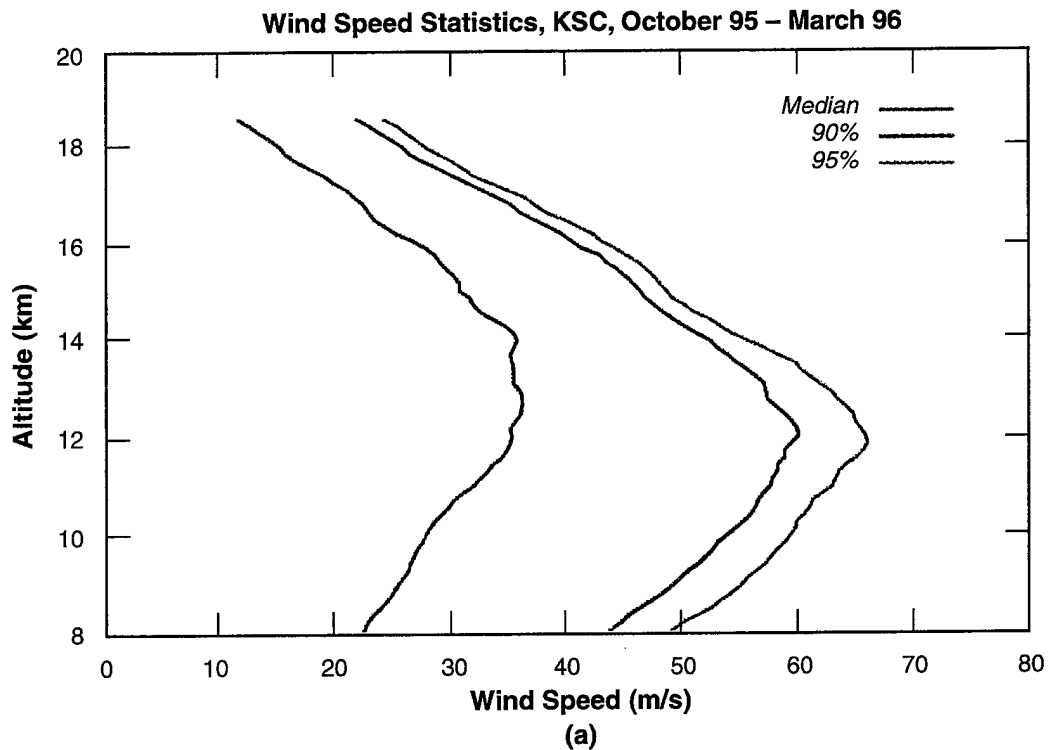
Figure 6. Profiles of (a) wind speed and (b) turbulence intensity statistics at Kennedy Space Center, Florida for the period October 1995 through March 1996. Left-most curves are (a) median wind speed and (b) median turbulence intensity. Curves to right are probability of exceedance limits, 90% (1-in-10) and 95% (1-in-20). Statistics developed from 50 MHz high power radar data of altitude resolution 150 m, one profile every 5 minutes for 183 days.

19

6. HIGH TURBULENCE INTENSITY CASES

Preliminary investigations are conducted for two known meteorological causes of severe turbulence: a) strong wind shear, as in the vicinity of jet streams, and b) strong convection, as near cumulonimbus clouds or thunderstorms. Considered are the physical mechanisms generating the high turbulence intensities and the methodologies for utilizing processed VHF radar data to quantify them.

The WSMR data were stratified to identify instances of the two meteorological conditions and extreme cases of each condition were selected: maximum and minimum wind shear and strong and weak convection. The six months of KSC data were searched and only extreme wind shear cases were selected. These occurred in the mid-winter period from January to March.

6.1 Wind Shear

The traditional theory for the origin of shear-type turbulence in the free atmosphere (above the surface boundary layer) relies upon spatial variation in the wind vector, especially the speed. High wind speed is the turbulence energy source and large wind speed gradients insure that eddies of very different speeds are in close proximity. The result is a large value of the spatial wind speed variance, σ_u^2 (m^2/s^2). This generates the characteristic fluctuations in the density of the atmosphere, i.e., in the refractive index, which is detectable by VHF radar.

Atmospheric wind shear, i.e., vertical wind speed change, is typically 10 to 100 times greater than the gradient in the horizontal. The strongest vertical shears are located in the vicinity of the jet streams where bands of maximum wind are located near the tropopause, or within layers that are both windy and thermodynamically stable. The greatest shears are expected in the layers just below and above the maximum wind speed at the core of jet streams or in stable high wind-shear layers where gravity wave breaking is occurring. Situations of especially strong wind shear were identified from the hourly wind profiles generated by the VHF radar data itself. All cases identified were jet-stream associated. Strong shear is considered as a vertical speed gradient of $\Delta U/\Delta z > 0.030$ s^{-1}, which means a wind speed change > 4.5 m s^{-1} from one 150 m range-gate to the next of the VHF radar data. The criterion for weak shear is $\Delta U/\Delta z < 0.005$ s^{-1}. Contrasting strong and weak cases are presented.

The cases of strongest, 'max', and also weakest, 'min', wind shear were selected based upon the rawinsonde observations, 00 and 12 UTC, taken at El Paso, Texas (~100 km from WSMR), and at Orlando, Florida (~100 km from KSC). For WSMR there were 3 max- and 2 min-shear cases during February 1993, and 2 max- and 2 min-shear cases during June 1991. For KSC, during the available period of the VHF radar record, there were 2 max- and 3 min-shear cases.

An example of a max-shear case from WSMR is given as Figure 7. Figure 7a contains the 20 individual wind speed profiles recorded during the 100 minutes 12:00 to 13:40 UTC (05:00-06:40 MST) at WSMR on 8 February 1993. A sharp jet maximum of 53 m s^{-1} occurs close to 11.7 km. Strong and nearly equal shear is found in the kilometer below and above the jet maximum. The corresponding turbulence intensity profiles are plotted in Figure 7b. The anticipation that maximum turbulence intensity

21

should correspond with maximum shear is borne out by the twin peak σ_u-values (maxima close to 3 m s^{-1}) precisely within the strong shear layers. Turbulence intensity maxima around 14.5 and 17 km may also be associated with substantial wind shear. At the core of the jet (just below 12 km), the shear, and therefore the vertical exchange of air parcels—the cause of detectable refractive index variations—is diminished and the turbulence intensity there is smaller. Comparison with the first and last panels of Figure 2a is suggested, along with reconsideration of their accompanying discussion.

Figure 7. Maximum wind shear case. Twenty individual profiles of (a) wind speed, and (b) turbulence intensity recorded at WSMR during the period 12.0 to 13.7 UTC, 8 February 1993.

22

Figure 8 is a minimum shear case from the WSMR data set, 7 June 1991, 12:00 to 13:40 UTC. The wind profiles were notably constant and featureless during this time period. The confined maxima in turbulence intensity near 12.7, 16.0, and 18.2 km are most likely due to specular reflection, a non-isotropic radar backscatter phenomenon related to thin isolated layers, rather than from isotropic turbulence originating from shear or convection.

The basic conclusion from the wind shear analysis is that VHF radar measurements support a definite 'positive' correlation between the magnitude of wind shear and turbulence intensity. The greater the vertical shear of the mean wind, the greater is the observed turbulence intensity, and vice-versa.

313486-8
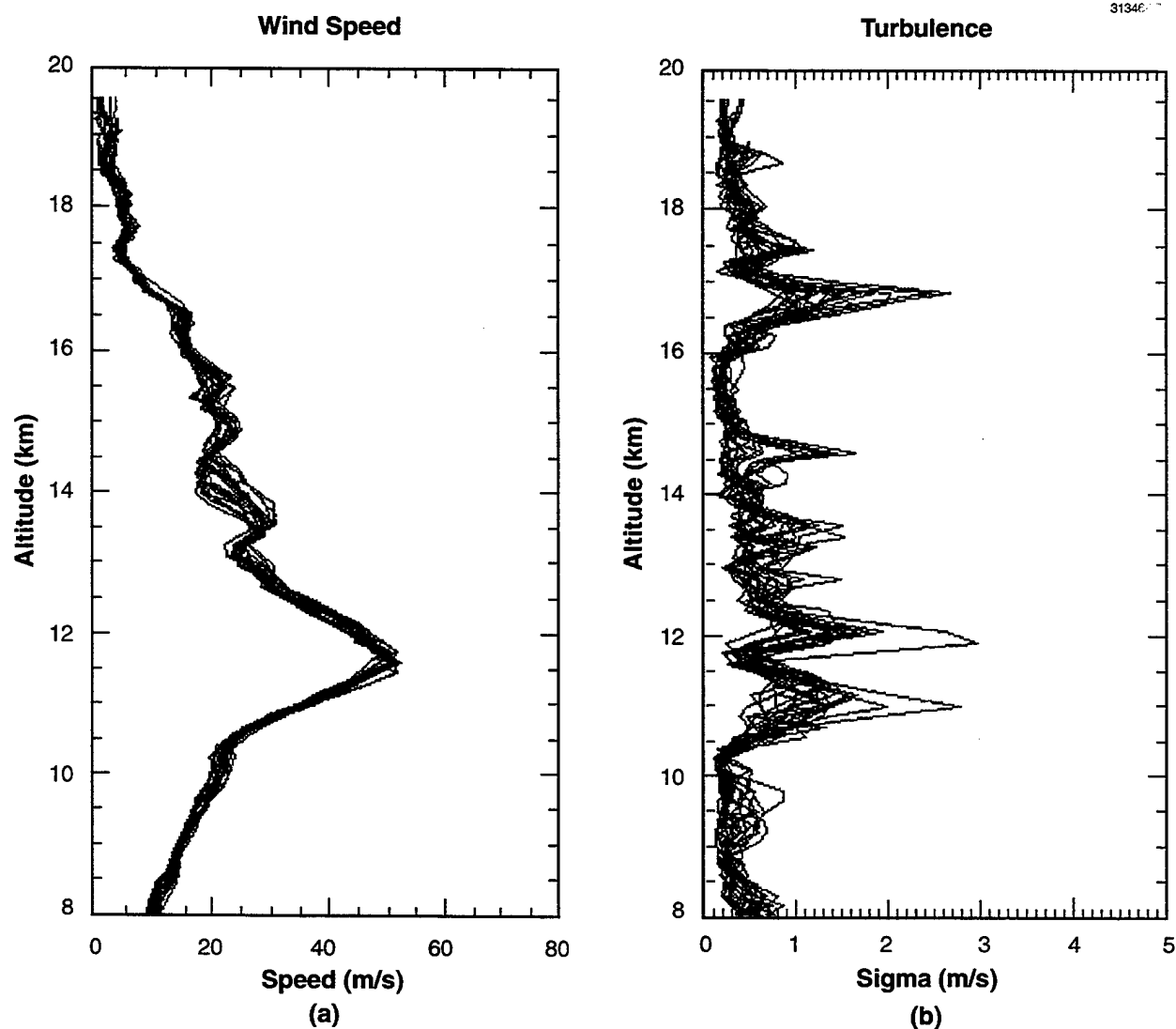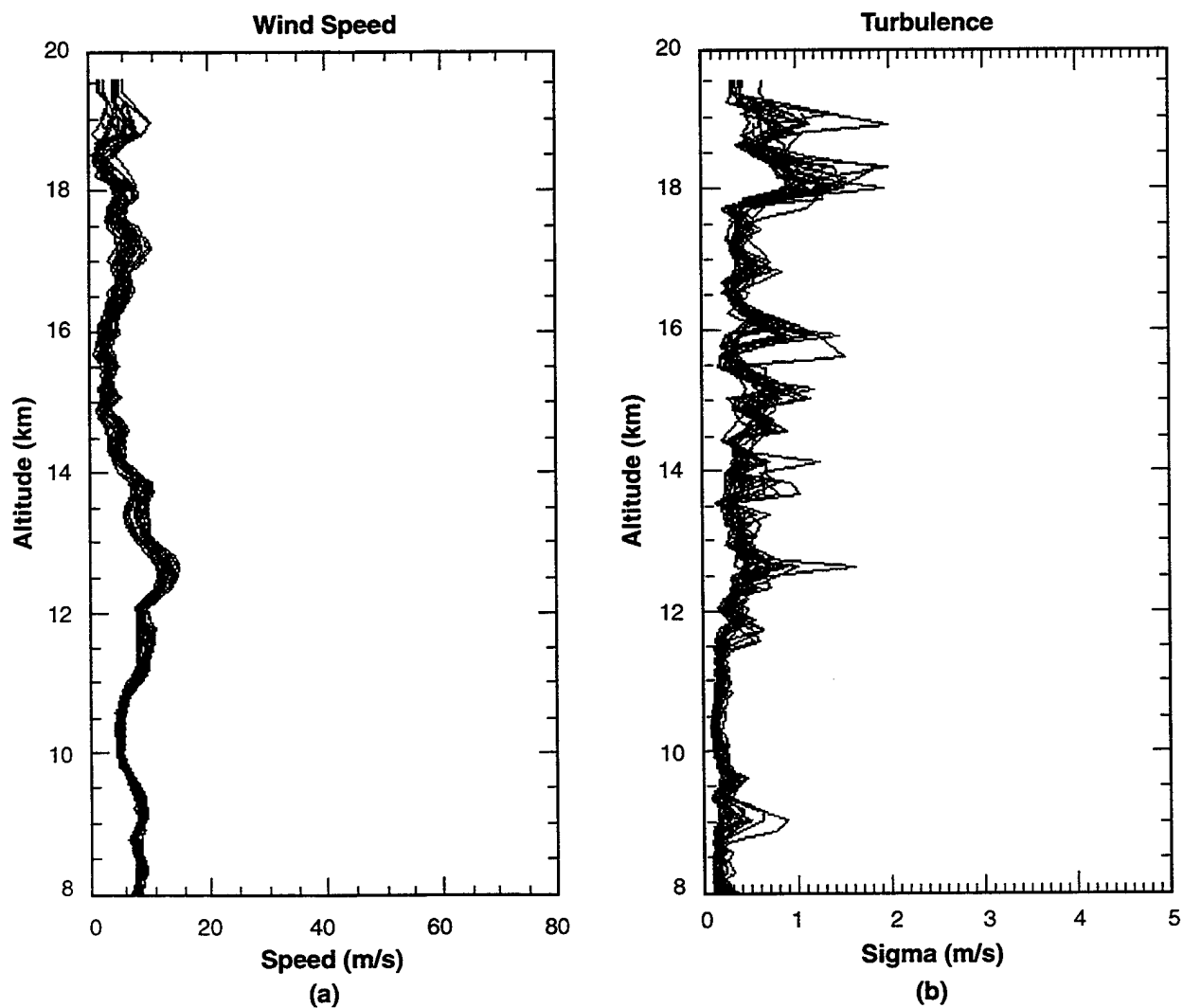
Wind Speed

Turbulence

Figure 8. Maximum wind shear case. Twenty individual profiles of (a) wind speed, and (b) turbulence intensity recorded at WSMR during the period 12.0 to 13.7 UTC, 7 June 1991.

23

6.2 Convection

Atmospheric turbulence is also known to be associated with convection within the troposphere, specifically, with the rapidly growing cumulonimbus clouds of thunderstorms. The associated turbulence is a recognized hazard to aviation. The source of the turbulent energy in this case is buoyancy, i.e., the temperature (density) of some parcels of air being higher (less) than the ambient value at a specific pressure level. During such situations, within the clouds themselves, the 'neutral' tropospheric lapse rate value of -6.5 K km^{-1} no longer prevails due to rapid latent heat release. Thermodynamic instability is present resulting in vertical motion, i.e., convection, which is sometimes vigorous. Also, water vapor, which is typically confined to the lower half of the troposphere, is then distributed throughout. All elements, such as the vigorous vertical motion, the water vapor presence, or both in combination contribute to a strong VHF radar signal.

The available VHF radar data were stratified into two contrasting classes: convective, also called 'unstable', and non-convective or 'stable'. The stratification was accomplished by analyzing the nearest coincident NOAA atmospheric radiosonde profile for thermodynamic instability. The common Showalter Index (SWI), a method for assessing the tendency of the troposphere to undergo vertical mixing, was used; SWI < 0 means unstable, SWI > 0 indicates stable. (The SWI is determined by comparison of the wet-bulb potential temperatures at two pressure levels, 850 and 500 mb.) The deep moist convection of thunderstorms is mainly a summer phenomenon and therefore only WSMR, June 1991 data are investigated for thermodynamic instability.

Figure 9 is an instance of an unstable troposphere (SWI = –1.5). The very high turbulence intensity values occurring below 10.5 km, in Figure 9b, are probably due mainly to contamination of the radar return by water vapor although vertical motion turbulence may also be present. This error cannot be eliminated from radar backscatter power without coincident water vapor profile data. Although the ϕ-method for turbulence assessment is not subject to such water vapor contamination (see Table A of the Appendix), the available WSMR data records are not complete enough to apply this type of turbulence analysis. Buoyancy-generated turbulence (from convective vertical motion), if present within the first 10.5 km of these WSMR data, cannot be isolated and quantified using the η-method. Between 10.5 and the tropopause near 12.5 km, the turbulence intensity is very low, ~0.2 m s^{-1}, which suggests that little convective activity is occurring below. The recurring maxima between 16 km and the top of the profiles are likely associated with wind shear.

A stable atmospheric situation is shown in Figure 10 (SWI = 7.1). No evidence of water vapor or convective vertical motion appears in the tropospheric turbulence intensity values. Within the middle stratosphere, specifically, above 17 km, the large intensity values are more likely due to specular reflection and low signal-to-noise, and not due to turbulent atmospheric motions.

24

Summarizing this initial convection analysis, it is generally true that low values of tropospheric instability result in low values of radar-observed turbulence intensity. However, high values of the convective activity index cannot be confidently correlated with high values of turbulence intensity as derived from the η-method, the radar backscatter power (C_n^2) analysis, due to its water vapor contamination problem. It is concluded that the ϕ-method should be applied when assessing turbulence intensity arising from moist convective activity.

313486-9

Figure 9. Convective (unstable) case. Twenty individual profiles of (a) wind speed, and (b) turbulence intensity recorded at WSMR during the period 00.0 to 01.7 UTC, 29 June 1991.

25

313486-10

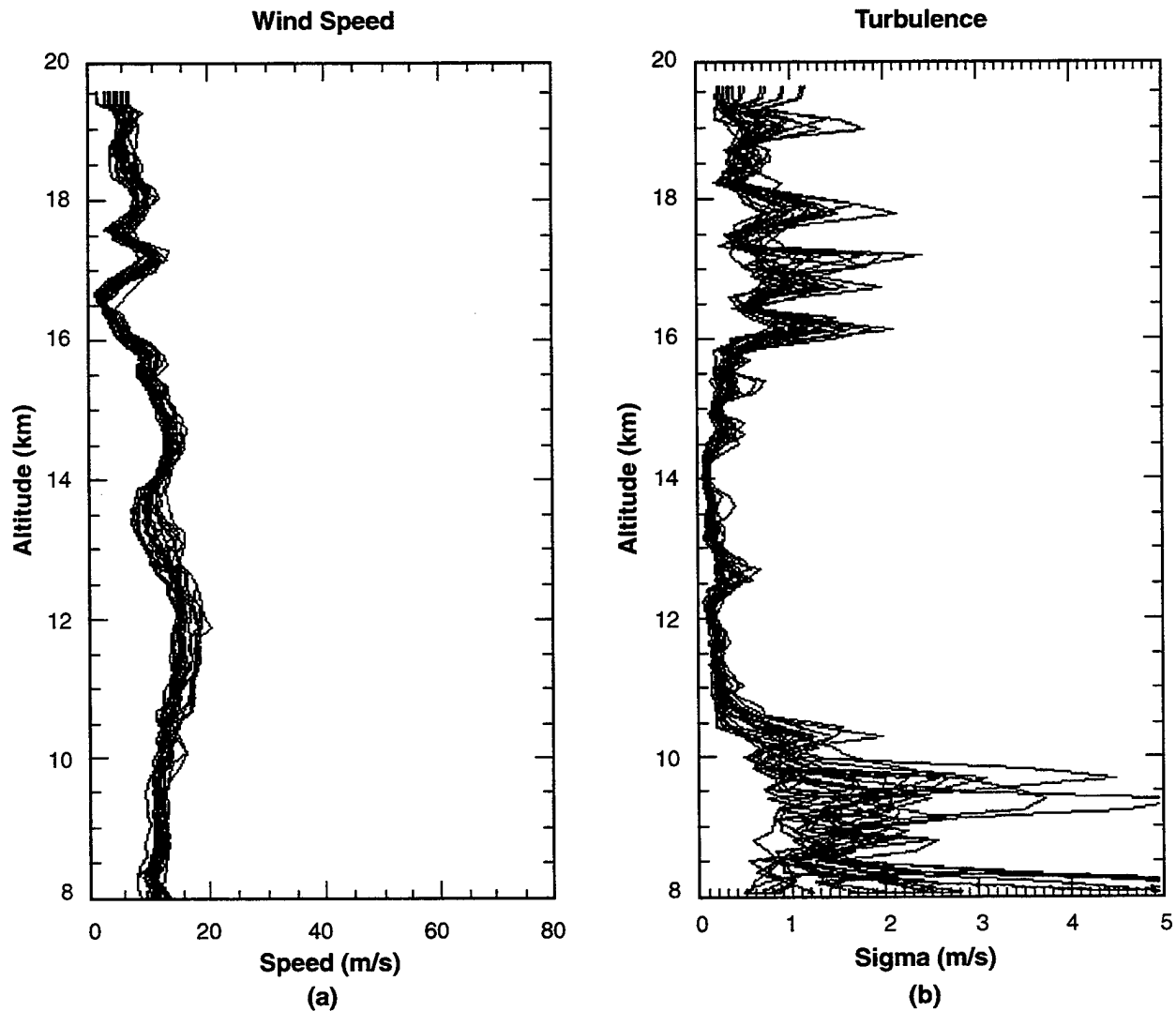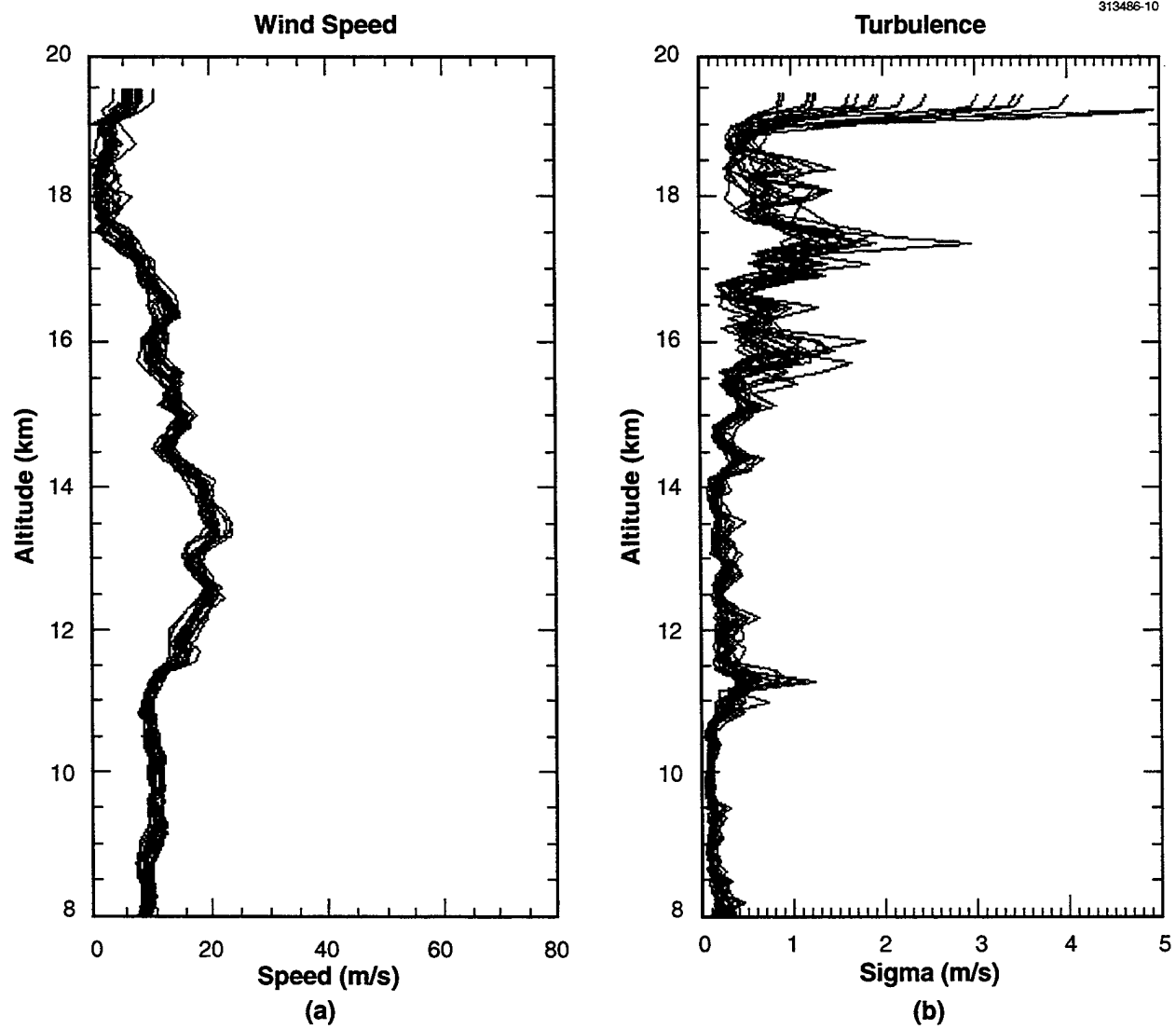*Figure 10. Non-convective (stable) case. Twenty individual profiles of (a) wind speed, and (b) turbulence intensity recorded at WSMR during the period 12.0 to 13.7 UTC, 15 June 1991.*

26

7. CLEAR-AIR TURBULENCE FORECAST

The Forecast Systems Laboratory (FSL) of NOAA has developed an algorithm to diagnose the location and intensity of clear-air turbulence (CAT), using the wind and thermodynamic fields predicted by the Eta numerical weather prediction (NWP) model. The FSL diagnostic algorithm applied to predicted fields is, then, a CAT forecast methodology. Three sources of turbulence are included in the algorithm: wind shear in the vicinity of jet streams, gravity wave breaking, and wind shear within 2 km of the surface, i.e., within the boundary layer. The first two are of interest in the present investigation.

The Eta model, as operated for the area of North America, has horizontal resolution of 29 km and variable vertical resolution. In the lower troposphere, but above the boundary layer, the vertical spacing of levels is 50 mb (approximately 500 m) but is close to 1.5 km in the vicinity of the tropopause. These resolutions are adequate to produce maps of CAT for a number of levels, some in the upper troposphere and lower stratosphere. Examples of the FSL CAT product for the United States are shown in Figure 11. The plotted variable is turbulent kinetic energy K (labeled TKE), which is $3/2\,\sigma_u^2$, since the isotropic condition is applicable (refer to Section 2). The comparable turbulence intensity used in this report is $\sigma_u = (2/3\ K)^{1/2}$.

The skill of the CAT forecast methodology has two major constraints: 1) the accuracy of the NWP scheme whose products are post-processed, and 2) the representation of turbulence physics in the algorithm itself. Relating to constraint 1, the quality of the Eta forecast wind and temperature fields is considered high, at least by environmental forecasting standards, and therefore the NWP constraint is minimized. However, within the free-atmosphere it has been determined that gridded fields of horizontal resolution better than 20 km and vertical separation not more than 500 m are needed to specify gravity-wave activity—this vis-à-vis the previously stated upper tropospheric resolutions of the Eta model, which is presently the best operationally available. Also, the Eta model is hydrostatic, whereas a breaking gravity wave, a complex shear-type turbulence producer, is a non-hydrostatic phenomenon.

Regarding constraint 2, the incorporation of turbulence physics in the diagnostic algorithm, boundary-layer turbulence theory is better developed than that of the free-atmosphere and is more fully included—to the credit of the FSL algorithm. The state of free-atmosphere turbulence theory could compromise the quality of the upper-tropospheric CAT products. On the other hand, free-atmosphere turbulence physics should be simpler, since it is not complicated by the overwhelming influence of a no-slip boundary or by the large effect of the diurnal heating cycle.

Another concern is that, unavoidably, Newton's 2nd Law applied to turbulent flow always has more unknowns than equations, requiring approximation of some unknowns in terms of otherwise known quantities (Stull, 1988, p. 199). However, the more equations explicitly treated, i.e., the higher the order of the moments-of-momentum expressions, the better the representation of the turbulence state. The level of 'closure' is the highest order of the momentum differential equation. The present CAT algorithm is referred to as a '1 1/2 order' closure scheme (Marroquin, 1996), i.e., the equations included are the mean wind component equations (1st order) and the turbulent kinetic energy equation in a 1/2-order, parameterized non-dissipative (K - ε) form (Stull, 1988, p. 219). Attempts so far to quantify the dependence of the

27

Figure 11a. Example of FSL's experimental CAT forecast data display at 25000, 30000, and 35000 feet on a relatively calm day (18 UTC, 20 November 1997). For isotropic turbulence $\sigma_u = (2/3TKE)^{1/2}$. Some areas have turbulence values (σ_u) exceeding 1.2 m/s. Only very limited spots have values exceeding 1.7 m/s.
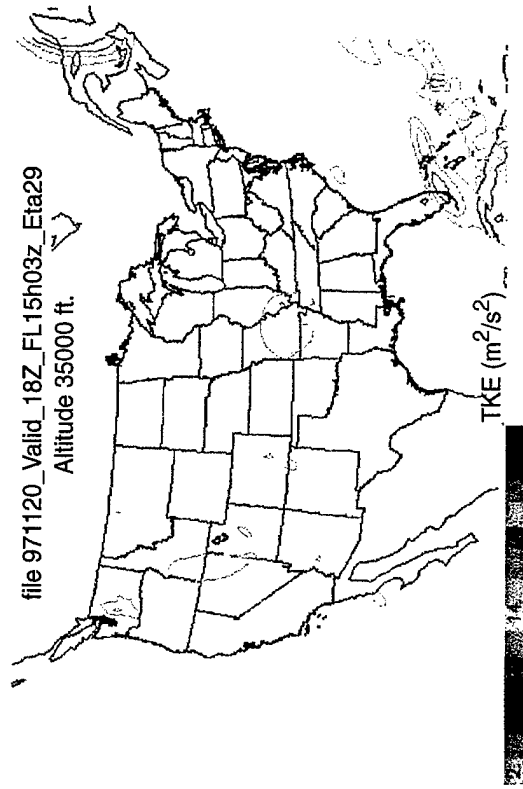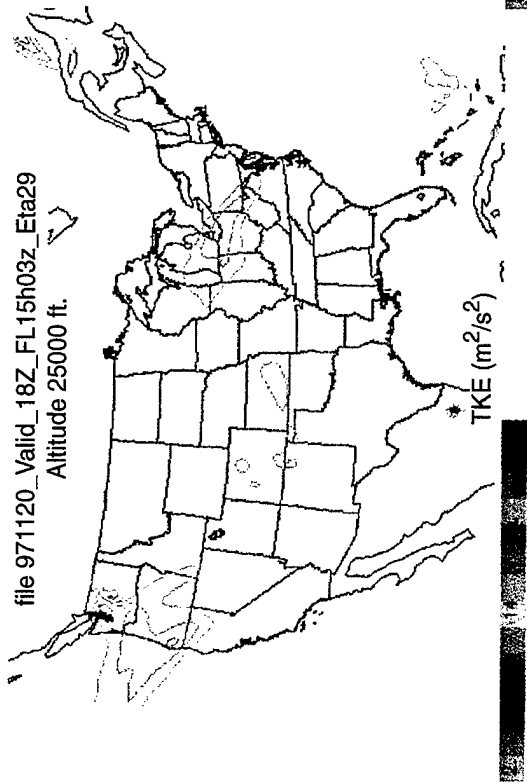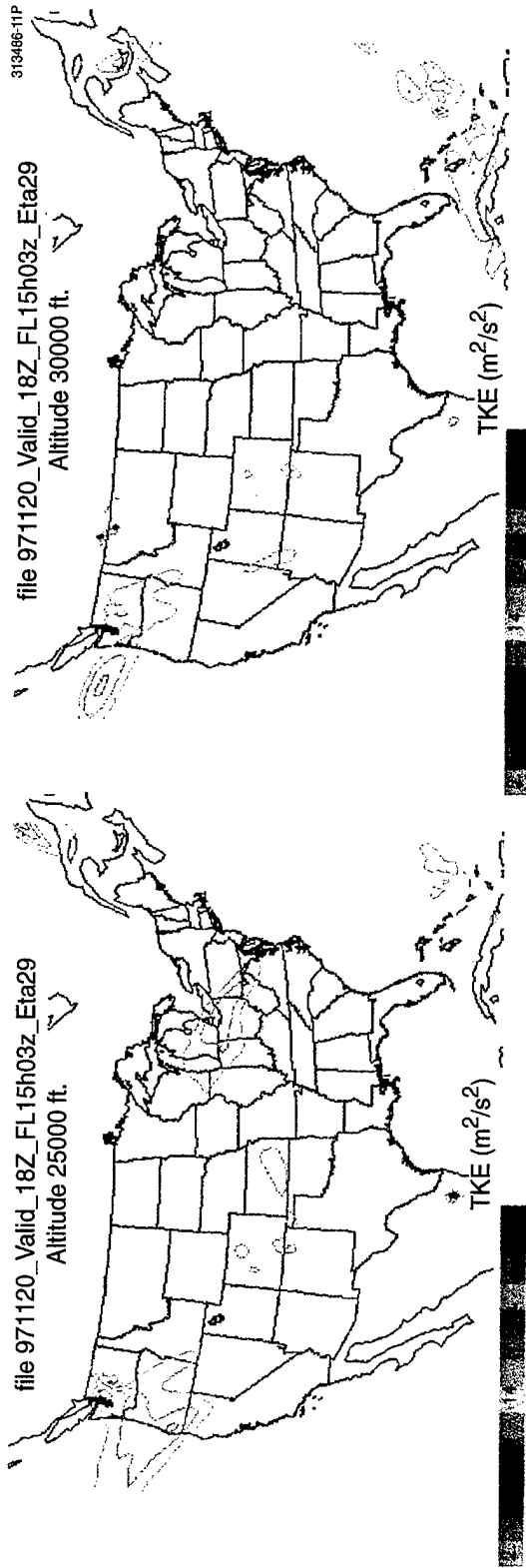
Figure 11b. Example of FSL's experimental CAT forecast data display at 25000, 30000, and 35000 feet on a turbulent day (15 UTC, 26 November 1997). For isotropic turbulence $\sigma_u = (2/3TKE)^{1/2}$. A considerable area has turbulence values (σ_u) exceeding 1.2 m/s. Some limited spots have $\sigma_u > 3.5$ m/s.

CAT algorithm on the level of closure have been frustrated by inadequate in-situ measurement, which are mostly the sporadic reports from transiting aircraft. While the 1 1/2 order-treatment of the turbulence physics is good, it is nevertheless incomplete, especially in such events as breaking waves. This may partially explain the CAT forecast false-alarm rate presently being experienced.

The FSL CAT forecast product, e.g., Figure 11, is unique. In spite of its relative newness and lack of long-term validation, it provides information on the preferred location and seasonal variation of turbulence in the free atmosphere. This type of turbulence information is available from no other source and could be used at least as guidance in extending and refining TEP statistics. In this regard, the FSL development algorithm could be applied to the output products of other NWP models, e.g., the European Center for Medium-Range Weather Forecasting (ECMWF) model, to widen the geographic coverage. There is a substantial role for VHF radar profile data, such as those used in Sections 5 and 6, in the substantial task of validating these CAT forecast products. Finally, the new CAT forecast clearly has immediate and practical application to civilian and DOD air operations.

8. CONCLUSIONS AND RECOMMENDATIONS

Modern high power Doppler VHF radar wind profilers are a valuable source of upper tropospheric turbulence intensity data. These radars can provide more comprehensive characterization of turbulence statistics than any in-situ measurement database, or even models developed from such databases. VHF radar provides continuous remote sensing of turbulence intensity as a function of height, called turbulence profiles, whereas in-situ measurement furnishes only sporadic, single-altitude observations. The short-coming for radar assessment of turbulence is the need to completely eliminate the effects of extraneous radar signal. This report has dealt specifically with VHF radar quantification of turbulence intensity, vis-à-vis the deficiencies of other turbulence intensity information sources. The methodologies reported on have been developed to retrieve turbulence intensity statistics from VHF wind profiler data.

8.1 Findings

Sample data sets from two high power radar profilers, located at WSMR, New Mexico, and KSC, Florida, were obtained and methodologies were developed for the retrieval of turbulence intensity statistics from such data. Summarizing the WSMR results, in the 8 to 20 km altitude region, the median turbulence intensity was found to be 0.5 m s^{-1}. In more turbulent conditions, the 90% and 95% TEP, turbulence intensities were observed to be close to, or slightly in excess of 1.0 m s^{-1} and 1.5 m s^{-1}, respectively. The KSC turbulence data analysis resulted in the median close to 1.0 m s^{-1}, the 90% TEP near 1.5 m s^{-1}, and the maximum 95% TEP of 1.7 m s^{-1}.

These initial findings, although only for short periods of time, may be compared with the published TEP profiles given in Figure 1. There, in the 8 to 20 km (26 to ~60 kft) altitude region, models for all TEP limits are seen as decreasing functions of altitude, the result of applying a factor $(\rho/\rho_0)^{1/2}$, where ρ is atmospheric density decreasing with altitude and ρ_0 is the standard atmosphere density at an appropriate reference level (AFWAL, 1982). The radar retrieved turbulence intensity profiles do not exhibit any similar decreases. Furthermore, the in-situ measured 10^{-2} (1-in-100) TEP in Figure 1 (bold curve) has an average value of 0.3 m s^{-1} (~0.8 ft/s), in the altitude region 8 to 11 km (26 to ~36 kft). From the VHF radar analyses, for the same altitudes, even the median intensity, the 50% (1-in-2) TEP, exceeds this average value by nearly a factor of 2 at WSMR (refer to Figures 3b and 4b), and a factor of 3 at KSC (Figure 6b).

The CAT forecast products developed by FSL can readily be analyzed to develop local-area and season-specific turbulence statistics and to predict turbulence intensities for operational purposes, at least in North America. With some adaptation, the CAT diagnostic algorithm could be applied to the output products of other global NWP forecast models to provide such turbulence intensity statistics globally.

8.2 Future Applications

More extensive TEP analyses of VHF radar data sets are feasible. There is a considerable archive of good-quality WSMR VHF data (1990–1995) and the WSMR radar is calibrated. Both backscatter-

power and spectrum-broadening methods could be applied to the WSMR record. The KSC VHF profile system has an ongoing mission in support of the NASA space launch facility. Its record began in 1990 and continues to the present. However, the KSC system is not calibrated and therefore only spectrum-broadening analysis, the η-method, is applicable for computing turbulence intensity statistics.

Two specific applications for available VHF wind profiler data are suggested: 1) more extensive investigation of severe turbulence events and 2) verification of CAT forecast products. In regard to application 1, very high turbulence intensity is expected when gravity waves break. This phenomenon, although rare, does occur in association with mountain ranges such as in the vicinity of WSMR and is extremely hazardous to air operations. The η-method is recommended for gravity wave research. Also, convective instability, associated with thunderstorms, is a more widespread source of significant turbulence and is common in the vicinity of KSC during the summertime. The ϕ-method is recommended for such investigations because of its insensitivity to water vapor presence. For application 2, the FSL forecast product is now routinely available for the continental United States. The data from high power VHF radar sites can provide the needed validation of this detailed spatial depiction of turbulence intensity.

REFERENCES (ANNOTATED)

1988:   Stull, R.B. An Introduction to Boundary Layer Meteorology. Kluwer Academic Publishers, Dordrecht, The Netherlands, 666 pp. (Atmospheric turbulence text.)

1972:   Meecham, W.C. Atmospheric Turbulence. Ch. 4 in: Remote Sensing of the Troposphere, V.E. Derr, editor, Wave Propagation Lab., NOAA. (Turbulence properties.)

1985:   Hocking, W.K. Measurement of Turbulent Energy Dissipation Rates in the Middle Atmosphere by Radar Techniques: A Review. Radio Sci., 1403–1422. (Considers the 2 turbulence analysis methods, η (C_n^2) & ϕ. T, q, & n fluctuations. Length scales in the inertial-subrange. Algorithms for determining ε.)

1972:   Hardy, K.R. Studies of the Clear Atmosphere Using High Power Radar. Ch. 14 in: Remote Sensing of the Troposphere, V.E. Derr, editor, Wave Propagation Lab., NOAA. (Theory and applications of scattering due to refractive index fluctuations.)

1961:   Tatarski, V.I. Wave Propagation in a Turbulent Medium. Dover Publications, Inc. New York, NY, 285 pp. (The original explanation of radar backscatter from $\Delta\rho$.)

1981:   LaBitt, M. Coordinated Radar and Aircraft Observations of Turbulence. Project Report ATC-108, MIT Lincoln Laboratory, Lexington, MA., 37 pp. (The relationship between C_n^2 and σ_u.)

1980:   Gage, K.S., J.L. Green, and T.E. VanZandt. Use of Doppler Radar for the Measurement of Atmospheric Turbulence Parameters From the Intensity of Clear-Air Echoes. Radio Sci., 407–416. (Important reference for η-method. Relationship of C_n^2 and σ_u.)

1978:   VanZandt, T.E., J.L. Green, K.S. Gage, and W.L. Clark. Vertical Profiles of Refractive Turbulence Structure Constant: Comparison of Observations by the "Sunset" Radar with a New Theoretical Model. Radio Sci., 819–829. (Important for backscatter power method. Model of C_n^2 (z) as function of profiles of U, T, q. Also, discussion of turbulent fraction F.)

1983a: Hocking, W.K. On the Extraction of Atmospheric Turbulence Parameters from Radar Backscatter Doppler Spectra – I: Theory. J. Atmos. Terr. Physics, 89–102.

1983b: Hocking, W.K. Mesospheric Turbulence Intensities Measured With a HF Radar at 35° S – II. J. Atmos. Terr. Physics, 103–114. (Application of the ϕ-method.)

1994:   NOAA/DOC. Wind Profiler Assessment Report – 1987-1994. National Weather Service, NOAA/DOC, Silver Spring, MD, 141 pp. (VHF profilers.)

1995:   Nastrom, G.D., and F.D. Eaton. Variations of Wind and Turbulence Seen by the 50 MHz Radar at White Sands Missile Range, NM. J. Appl. Meteor., 2135–2148.

1995:   Nastrom, G. D. Variability of C_n^2 and Wind as Seen by the 50 MHz Radar at White Sands Missile Range, NM. ARL-CR-197, Atm. Research Lab., WSMR, NM, 54 pp.

1992:   ENSCO. Preliminary Report on the Implementation of the New Wind Algorithm in NASA's 50 MHz Doppler Radar Wind Profiler. ENSCO, Inc., Melbourne, FL, 66 pp.

1996:   Marroquin, A. Verification of Algorithms to Forecast Clear-Air Turbulence (CAT). Proc. of 33rd Aerospace Meeting on Atmospheric Turbulence, AIAA, Reno, NV, 1–8.

1982:   AFWAL/AFSC. Background Information and User Guide for MIL-F-8785C, Military Specification – Flying Qualities of Piloted Airplanes. AFWAL-TR-81-3109, Flight Dynamics Laboratory, AF Wright Aeronautical Labs, Wright-Patterson AFB, OH, 176 pp. (Documentation of TEP diagram development.)

1990:   Vernin, J., M. Crochet, M. Azouit, and O. Ghebrebrhan. SCIDAR/Radar Simultaneous Measurements of Atmospheric Turbulence. Radio Sci., 953–959. (Demonstration of the impact of water vapor profiles on C_n^2.)

1996:   Nastrom, G.D. Doppler Radar Spectral Width Broadening Due to Beamwidth and Wind Shear. (Unpublished manuscript.)

APPENDIX—ERROR SOURCES

Table A-1 lists the recognized error sources for turbulence assessment using VHF radar wind profilers: 1) the η-method and 2) the φ-method. Whether the source is due to environmental factors or radar system parameters, the effect is always a reduction in the signal-to-noise ratio. Generally, the error sources are fewer and can be more correctly specified for the φ-method. However, their magnitudes are usually larger than those affecting the η-method. The η-method, on the other hand, requires calibration of the radar.

TABLE A-1

Error Sources in VHF Radar Determined Turbulence Intensity (σ_u)

Spectrally Integrated Backscatter Power, the C_n^2 or η-Method*	Spectrum Width Broadening, the φ-Method**
1. Water vapor presence, esp below 8 km	1. Specular reflection from thin stratified layers
2. Vertical temperature gradient near zero	2. 'Beam' broadening (finite beam width & U)
3. Vertical temperature gradient > adiabatic	3. 'Shear' broadening (finite range interval, h)
4. Insufficient radar calibration	4. 'Temporal' broadening (integration time)
5. Fraction of radar volume turbulent	5. Actual U(t) (for very long integration times)
6. Specular reflection (near-vertical beam)	6. Gaussian assumption for spectrum shape
7. Temporarily out of inertial subrange	7. Gravity wave effect (change in w within h)
8. Convective activity	
* Major sources in 8–12 km region are 1–5.	** Major sources in 8–12 km region are 1–3.

A.1 Principal η-Method Errors

The presence of water vapor has a large impact (as much as a factor of 50) on scattered radar energy η and therefore on the value of C_n^2 (Vernin et al., 1990, pp. 955, 956). It is a major error source in the η-method. Although elimination of this effect is conceptually straightforward, given the expression for the atmospheric index of refraction equation (Tatarski, 1961, p. 55, Eq. 3.44), high-resolution and coterminous profiles of atmospheric water vapor content, determined independently, are required. Such data are rarely available and therefore reliable turbulence intensity quantification cannot be obtained using the η-method below about 7 or 8 km in mid-latitude regions. Also, the presence of deep moist convection (cumulonimbus clouds) can preclude reliable turbulence intensity retrievals even in the upper troposphere due to the presence of water vapor (refer to Section 6.2).

35

The vertical temperature gradient, expressed in terms of the Brunt-Vaisala frequency, is found in the denominator of the expression for the turbulent energy dissipation rate ε and it may approach zero in thin layers of the troposphere. In such localized situations the η-method retrieval is unreliable. Compromising vertical resolution by averaging or adopting representative 'constant' values (as done here) are strategies to avoid over-estimations.

A.2 Principal ϕ-Method Errors

Specular reflection is an error source for either method, but is a major contaminant of the Doppler spectrum data. It is caused by a vertically thin turbulent sub-layer persisting within an otherwise very stable atmospheric layer and having step-change boundaries which inhibit its dissipation. The returned signal caused by this phenomenon is localized around a single frequency and the power is far above the otherwise near-Gaussian spectrum. Therefore, this error can readily be eliminated — manually or by algorithm. Graphic examples of the effects of specular reflection on spectra are given in Hocking (1983b, pp. 105, 106, Figures 3 and 4). This error is especially prevalent at zenith and can be reduced by increasing the off-zenith angle.

Regarding corrections specific to the ϕ-method of turbulence intensity quantification, three Doppler spectrum broadening mechanisms are distinguished. Each results from relationships between radar system parameters, such as finite beamwidth, and environmental factors. The interrelations lead to spurious spectrum broadening which must be quantified and subtracted from the measured spectrum width, as indicated in Section 4.2. The three spurious effects are beam, shear, and temporal broadening, and are discussed by Hocking (1983a, p. 92, Figures 2 and 3).

Beam broadening results from a mean wind speed across the finite angular width of any beam, orientated at any angle. This combination results in Doppler shifting to higher frequencies along the upwind side of the beam, and to lower frequencies along the downwind side. The effect is eliminated by knowing beam width, tilt angle and mean wind velocity (speed and direction). An expression for eliminating this effect is given by Nastrom (1996, Eq. 16).

Shear broadening results from vertical variation in the mean wind speed within the finite range interval of a beam pointing off-zenith. This combination leads to shifting in the vertically higher portion of the range interval which is different from that in the lower portion of the tilted beam range volume. The environmental wind profile and radar range-volume dimensions are needed to correct for this spurious broadening. Nastrom (1996) provides the terms necessary for eliminating this type of broadening. The effects of beam and shear broadening are not separable and the expression for the resulting error portion of the variance is: $\sigma_e^2 = [(\lambda/2)^2 \, (\phi_e^2)]/2 \ln (2)$.

Temporal broadening results from the need for sampling over a reasonable amount of time in order to generate the spectrum of turbulence fluctuations. Gravity waves, which mainly propagate horizontally in the troposphere and vertically in the stratosphere, will then contribute to the broadening of the spectrum width. Unless gravity wave activity is otherwise detected, the mitigation strategy is to minimize the integration time (1 min for data used here is a short time).

36

REPORT DOCUMENTATION PAGE			Form Approved OMB No. 0704-0188

Public reporting burden for this collection of information is estimated to average 1 hour per response, including the time for reviewing instructions, searching existing data sources, gathering and maintaining the data needed, and completing and reviewing the collection of information. Send comments regarding this burden estimate or any other aspect of this collection of information, including suggestions for reducing this burden, to Washington Headquarters Services, Directorate for Information Operations and Reports, 1215 Jefferson Davis Highway, Suite 1204, Arlington, VA 22202-4302, and to the Office of Management and Budget, Paperwork Reduction Project (0704-0188), Washington, DC 20503.

1. AGENCY USE ONLY (*Leave blank*)	2. REPORT DATE 25 September 1998	3. REPORT TYPE AND DATES COVERED Technical Report	

4. TITLE AND SUBTITLE

Radar Determination of Turbulence Exceedance Probability

6. AUTHOR(S)

J. William Snow, Hsiao-hua K. Burke, Daniel C. Peduzzi, Carolyn A. Upham, and Michael P. Jordan

5. FUNDING NUMBERS

C — F19628-95-C-0002

7. PERFORMING ORGANIZATION NAME(S) AND ADDRESS(ES)

Lincoln Laboratory, MIT
244 Wood Street
Lexington, MA 02420-9108

8. PERFORMING ORGANIZATION REPORT NUMBER

TR-1049

9. SPONSORING/MONITORING AGENCY NAME(S) AND ADDRESS(ES)

DARPA/ISO
2701 North Fairfax Drive
Arlington, VA 22203-1714

10. SPONSORING/MONITORING AGENCY REPORT NUMBER

ESC-TR-97-116

11. SUPPLEMENTARY NOTES

None

12a. DISTRIBUTION/AVAILABILITY STATEMENT

Approved for public release; distribution is unlimited.

12b. DISTRIBUTION CODE

13. ABSTRACT (*Maximum 200 words*)

Modern high power Doppler VHF radar wind profilers are a valuable source of upper tropospheric turbulence intensity information. These radars can provide more comprehensive characterization of turbulence statistics than any in-situ measurement database, or even models developed from such databases. Sample data sets from two high power radar profilers, located at WSMR, New Mexico, and KSC, Florida, were obtained. The physical processes involved in turbulence production, maintenance, and dissipation were reviewed along with the phenomenology of its detection using radar. Subsequently, methodologies were developed for the retrieval of turbulence intensity statistics, or the so-called turbulence exceedance probabilities (TEP), from such data. The WSMR data analysis shows that, in the 8 to 20 km altitude region, the median turbulence intensity was ≤ 0.5 m s^{-1}. In more turbulent conditions, the 90% and 95% TEP, turbulence intensities were observed to be close to, or slightly in excess of 1.0 m s^{-1} and 1.5 m s^{-1}, respectively. The KSC turbulence data analysis resulted in the median close to 1.0 m s^{-1}, the 90% TEP near 1.5 m s^{-1}, and the maximum 95% TEP of 1.7 m s^{-1}.

Also considered are the capabilities of a recently developed Clear Air Turbulence (CAT) forecast product. The conclusion is that available TEP guidance could be validated and extended by analysis of data from high power radars.

14. SUBJECT TERMS

15. NUMBER OF PAGES
48

16. PRICE CODE

17. SECURITY CLASSIFICATION OF REPORT Unclassified	18. SECURITY CLASSIFICATION OF THIS PAGE Same as Report	19. SECURITY CLASSIFICATION OF ABSTRACT Same as Report	20. LIMITATION OF ABSTRACT Same as Report

NSN 7540-01-280-5500

Standard Form 298 (Rev. 2-89)
Prescribed by AMSI Std. 239-18
298-102